Carbon 111 (2017) 467–475

Contents lists available at ScienceDirect

Carbon

journal homepage: www.elsevier.com/locate/carbon

Ti/Al co-doping induced residual stress reduction and bond structure evolution of amorphous carbon films: An experimental and ab initio study

Xiaowei Li [a, *], Peng Guo [a], Lili Sun [a, b], Xiao Zuo [a], Dong Zhang [a], Peiling Ke [a], Aiying Wang [a, **]

[a] Key Laboratory of Marine Materials and Related Technologies, Zhejiang Key Laboratory of Marine Materials and Protective Technologies, Ningbo Institute of Materials Technology and Engineering, Chinese Academy of Sciences, Ningbo, 315201, PR China
[b] University of Chinese Academy of Sciences, Beijing, 10049, PR China

ARTICLE INFO

Article history:
Received 15 July 2016
Received in revised form
2 September 2016
Accepted 15 October 2016
Available online 17 October 2016

ABSTRACT

Amorphous carbon (a-C) films co-doped by two metals exhibit a desirable combination of mechanical and tribological properties for wider applications. Nevertheless, the structural evolution of metal co-doped a-C films from the atomic and electronic scales is a critical pre-requisite to illustrate the intrinsic mechanism of residual stress reduction. Herein, we first fabricated the Ti/Al co-doped a-C films with different concentrations by a hybrid ion beam system. When the co-doped Ti/Al concentrations were $<Ti_{3.9\ at.\%}/Al_{4.4\ at.\%}$, the Ti and Al atoms were dissolved in the a-C matrix without forming a carbide phase; with the Ti/Al concentrations further increased beyond of $Ti_{3.9\ at.\%}/Al_{4.4\ at.\%}$, the crystalline titanium carbide nano-particles appeared, while Al existed in the form of aluminum oxidation state in the films. The residual stress, hardness and elastic modulus of films were strongly dependent on the chemical state of the co-doped Ti/Al atoms, which decreased first and then increased with Ti/Al concentrations. Ab initio calculations revealed that the residual stress reduction in a-C films caused by Ti/Al co-doping was mainly attributed to the significant relaxation of distorted C—C bond lengths and the formation of a weak covalent interaction for Ti—C bonds and the ionic interaction for Al—C bonds.

1. Introduction

Amorphous carbon (a-C) films open a wide field of applications for functional coatings with tailored mechanical, tribological, biological and optical properties due to their excellent high hardness, low coefficient of friction, chemical inertness, good biocompatibility and optical transparency [1–3]. In particular, doping metal into a-C films has been considered as an effective strategy to control the film properties and to optimize e. g. friction and electronic behaviors for the applications of cutting tools, automobile components, magnetic disk storage and vascular stent [4–7]. For example, metal dopants in a-C matrix could bring the considerable reduction of intrinsic residual compressive stress due to the promoted graphitization of C-sp^2 bonds [8], substitution of strong C—C bonds by weak Me—C bonds [9], or pivot site of metal nanoparticulates for structure relaxation [10]. If one keeps in mind the different feature of doped metals, it thus would be very interesting to explore new performance/functions conveyed by multiple coexisting dopants. However, previous works mainly focused on mono-doping with various chemical elements such as Si, Ti, Cr, Al, Ag etc [11–14], but up to now only few studies on duplex co-doped a-C films are presented.

Recently, Liu et al. [15,16] reported that compared with Ti-doped a-C films, the introduction of Al synergistically enhanced the graphitization of carbon films and thereafter lowered the residual stress; in addition, the co-doped films also exhibited the high toughness, low coefficient of friction and wear rate due to the formed nanocomposite structures. Moreover, when Ti was replaced by Si, a Si/Al co-doped a-C film with dual or hierarchy nanostructure constructed of cross-linking networks and fullerene-like structures was obtained, which exhibited extremely high elasticity, super low friction and superior wear resistance [17]. These results bring forward a new concept to design a-C films with desirable

* Corresponding author.
** Corresponding author.
E-mail addresses: lixw@nimte.ac.cn (X. Li), aywang@nimte.ac.cn (A. Wang).

http://dx.doi.org/10.1016/j.carbon.2016.10.033
0008-6223/

combination of mechanical, tribological and even other functional properties by taking fill advantages of the synergistic effect from co-doped metals. Nevertheless, a comprehensive understanding of the role of co-doped metal elements on the relationship between structure and properties is still required. Most importantly, due to the difficulties in direct observation of structural evolution by experiments with atomic and electronic scales and the complexity of co-doped metal natures, the dependence of residual stress on microstructure has not been fully understood yet, which is essential and significant to explore the stress reduction mechanism and deposit the thicker a-C films with high performance for friction components. Ab initio calculations provide a robust method to capture the atomic and electronic details and gain a deeper insight into the stress reduction mechanism of metal co-doped a-C films [18,19].

In this work, we used a unique hybrid ion beam system to fabricate the Ti/Al co-doped a-C films with different Ti/Al concentrations. Compared to the traditional reactive magnetron sputtering [15–17], PE-CVD [20] and cathodic vacuum arc techniques [21], the hybrid ion beam system comprising a DC magnetron sputtering unit and an anode-layer linear ion beam source (ALIS) can not only easily tailor the metal concentrations in a large range and the intrinsic structure of films, but also realize the high ionization rate and kinetic energy of C_2H_2 carbon source and the large-area uniformity of a-C films, representing the low-cost, facile advantages for mass production technique [22,23]. The in-depth analysis of composition, microstructure and mechanical properties was carried out according to the comprehensive experimental and theoretical methods. Most importantly, the simplified Ti/Al co-doped amorphous carbon networks were constructed by ab initio calculations, and the effect of co-doped Ti/Al on the bond structure evolution from the atomic and electronic scales was investigated to illustrate the fundamental mechanism of residual compressive stress reduction. It was observed that the residual stress and mechanical properties were strongly sensitive to the chemical state of co-doped Ti/Al atoms and the microstructure evolution caused by Ti/Al co-doping.

2. Experimental and calculation details

2.1. Experimental details

2.1.1. Film deposition

The a-C films with different Ti/Al concentrations were prepared by the unique hybrid ion beam deposition system consisting of a DC magnetron sputtering with Ti/Al composite target and an ALIS supplied with C_2H_2 gas for a-C film deposition [24,25]. A p-type Si (100) wafer with thickness 450 ± 20 μm was used as substrate, and a thin one with thickness of 240 ± 5 μm was also used as substrate to accurately estimate the residual stress. All substrates were cleaned ultrasonically in acetone, ethanol, and dried in air blow before putting into the vacuum chamber. The distance from the substrate to the ALIS and Ti/Al target was controlled about 20 cm separately. Prior to deposition, the chamber was evacuated to a vacuum of 2.7×10^{-3} Pa, and the substrates were pre-cleaned for 10 min using Ar^+ ions (Ar flow rate of 40 sccm) at the bias voltage of −100 V. During film deposition process, the working pressure was kept at 0.56 Pa; C_2H_2 gas with the flow rate of 10 sccm was introduced into the ALIS to obtain the hydrocarbon ions, and the working current and voltage of the ALIS were 0.2 A and 1400 ± 50 V, respectively; Ar sputtering gas flow with 70 sccm was supplied to the magnetron sputtering source, where a Ti/Al composite target with the Ti/Al atomic rate of 1:1 was used. The low concentration of co-doped Ti/Al in films was controlled by changing the sputtering current from 1 to 4 A. A negative pulsed bias voltage of −50 V (350 KHz, 1.1 μs) was applied to the substrate during film deposition. The deposition time was 1 h, but for the deposited films the effect of film thickness on structural properties was neglected because Fig. S1 in Supporting Information revealed that no significant change was observed with thickness increased from 400 to 1200 nm.

2.1.2. Film characterization

A surface profilometer (Alpha-step IQ, USA) was used to measure the thickness of the deposited films with employing a step formed by a shadow mask. X-ray photoelectron spectroscopy (XPS, Thermo Scientific ESCALAB 250) with Al X-ray source was used to characterize the composition and chemical bonds of the deposited films. Before commencing the measurement, the sample surface was etched by Ar^+ ion beams with energy of 3 keV for 5 min to remove the contaminants; the Ti/Al/C atomic ratio of the films was determined based on the atomic sensitivity factors and area ratio of the C 1*s* to Ti 2*p* and Al 2*p* peaks in XPS spectra of the films, and the hydrogen atom concentration was not considered due to its signal intensity below the XPS detection threshold. In addition, Raman spectroscopy (RenishawinVia-reflex) equipped with a He-Ne laser of 532 nm exciting wavelength was employed to further evaluate the carbon atomic bonds at a detecting range from 800 to 2000 cm^{-1}. The surface morphology of the films was studied by AFM (Dimension 3100 V, Veeco, US) at a scan rate of 2.0 Hz. The root-mean-square roughness R_q of the film surfaces was calculated from 512 × 512 surface height data points obtained from 1 μm × 1 μm scan area. Cross-sectional high-resolution transmission electron microscopy (TEM) of the films was performed on Tecnai F20 electron microscope, which was operated at 200 keV with a point-to-point resolution of 0.24 nm.

Mechanical properties were measured by a MTS-G200 nanoindenter tool in a continuous stiffness measurement mode with a maximum indentation depth of 500 nm and a Berkovich diamond tip. The characteristic hardness of the films was chosen in the depth where the hardness with indentation depth was stable and was not affected by the substrate. Six replicate indentations were done for each film. The residual stress was calculated according to the Stoney equation and the curvature of the film/substrate was determined by a laser tester (JLCST022, J&L Tech).

2.2. Calculation details

All the calculations were carried out using the Vienna ab initio simulation package based on density functional theory [26,27]. The initial configuration contained 60 atoms in a simple cubic supercell under periodic boundary conditions throughout the simulation. To model Ti/Al co-doped a-C films, a two-step process composed of melt-quenching by ab initio molecular dynamics (AIMD) simulation and geometric optimization (GO) was used [19,28–30]. During the AIMD simulation, the initial sample was first equilibrated at 8000 K for 1 ps to become completely liquid state and eliminate its correlation to the initial configuration using *NVT* ensemble with a Nose thermostat for temperature-control and a time step of 1 fs; then, in order to provide more representative models than the direct substitution of carbon by metal atoms in pre-generated pure carbon networks, Ti and Al atoms were introduced into sample by substituting carbon atoms in the liquid carbon state with a external equilibrium at 8000 K for 0.5 ps; after that, the sample was quenched from 8000 to 1 K at cooling rate of 1.6×10^{16} K/s. For the subsequent GO of amorphous structure, atomic relaxation based on conjugated gradient method was repeated until the forces acting on the atoms were below 0.01 eV/Å, and a self-consistent field was created using an energy convergence criterion of 10^{-5} eV. The detailed calculation process could refer to the previous study [19].

In addition, during the calculation, the cutoff energy was 500 eV, the exchange-correlation was handled in the generalized gradient approximation with the Perdew-Burke-Ernzerhof parameterization [31], and a gamma point only was used to sample the Brillouin zone.

3. Results and discussion

3.1. Thickness and composition

Table 1 shows the thickness and Ti/Al/C concentrations in the films deposited at different sputtering currents. It can be seen that as the sputtering current changes from 1 to 4 A, the thickness increases from 702 to 1371 nm monotonously, indicating the growth rate varied from 11.7 to 22.8 nm/min, which is similar to the previous results in Ti or Al mono-doped a-C films [8,24,32]. The Ti/Al concentrations with sputtering current also increase gradually following the decrease of the C concentration; when the sputtering current is 2.5 A, the Ti/Al concentrations are $Ti_{3.9\ at.\%}/Al_{4.4\ at.\%}$, while they reach to $Ti_{8.5\ at.\%}/Al_{14.4\ at.\%}$ in the film deposited at 4 A. The increased sputtering current enhances the bombardment effect of Ar ion on the Ti/Al composite target, so more Ti and Al atoms are sputtered from the target to deposit on the substrate, resulting in the increase of growth rate and Ti/Al concentrations in films. Especially, noted that the Al concentration for each film is higher than that of Ti due to the higher sputtering yield of Al atoms [16]. For the film deposited at the sputtering current of 1 A, Ti and Al atoms cannot be detected by XPS due to the existing target poisoning and lower energy of incident Ar ions which cannot overcome the sputtering threshold value of Ti/Al composite target.

3.2. Microstructure

Fig. 1 displays the typical XPS results of films with different Ti/Al concentrations including Al 2*p*, Ti 2*p*, and C 1*s* spectra. The XPS survey spectra are provided as Fig. S2 in Supporting Information for reference. The Al 2*p* XPS spectra shown in Fig. 1a illustrate an Al—O peak with binding energy of 74 eV and the peak intensity increases with Al concentration in the films, implying that the doped Al atoms in carbon matrix exist in the form of aluminum oxidation state [24]. The formation of oxidized aluminum may result from the rest of O_2 or H_2O during the plasma deposition process due to the insufficient vacuum. Similar to the evolution of Al, the intensity of Ti 2*p* peak in Fig. 1b increases with Ti concentration as well. Despite the changes occurred in the peak intensity, however, no significant variations can be elucidated from the spectra of Ti 2*p* peaks in films because it is rather difficult to distinguish the chemical bond between the metallic Ti and Ti carbide. According to the evolution of C 1*s* spectra (Fig. 1c), there is a major peak located at 284.6 eV for all films, representing the typical binding energy of a-C films [33], and the intensity of C 1s peak as a function of the Ti/Al concentrations decreases gradually as a consequence of the decreased C concentration in the films.

To further investigate the atomic bond structure in films, we take the $Ti_{3.9\ at.\%}/Al_{4.4\ at.\%}$ co-doped a-C film for representative example (Fig. 1d). The C 1*s* peak can be deconvoluted into four components with binding energies at 284.6 eV for C—C/C—H bond, 286.6 eV for C—O bond, 288.7 eV for C═O bond, and 282.1 eV for a small shoulder peak resulted from the C—Ti bonds [11,32], respectively. As the Ti/Al concentrations increase to $Ti_{8.5\ at.\%}/Al_{14.4\ at.\%}$, the peak intensity of C—Ti bond becomes more obvious (Fig. 1c), indicating higher fraction of formed titanium carbide. Nevertheless, there is no shoulder peak for C—Ti bond observed as the Ti/Al concentrations are less than $Ti_{3.9\ at.\%}/Al_{4.4\ at.\%}$, which means the doped Ti atoms do not bond with the carbon atoms to form titanium carbide. In addition, neither aluminum carbide peak (around 281.5 eV) nor aluminum oxycarbide (around 282.5 eV) is detected in the C 1s spectra of the films regardless of the Ti/Al concentrations [12,34]. As a result, it could be said that when Ti/Al concentrations are larger than $Ti_{3.9\ at.\%}/Al_{4.4\ at.\%}$, the doped Ti atoms with higher concentration begin to bond with carbon atoms and form the titanium carbide phase, but the doped Al atoms only exist as aluminum oxidation state for each case.

Fig. 2 shows the cross-sectional TEM and AFM results of the films with $Ti_{0.4\ at.\%}/Al_{0\ at.\%}$, $Ti_{3.9\ at.\%}/Al_{4.4\ at.\%}$ and $Ti_{8.5\ at.\%}/Al_{14.4\ at.\%}$, respectively. It can be seen that for the film with $Ti_{0.4\ at.\%}/Al_{0\ at.\%}$, the corresponding selected area electron diffraction (SAED) in Fig. 2a illustrates a broad and diffuse diffraction halo, indicating a typical amorphous character, and the co-doped Ti/Al dissolve in the amorphous carbon matrix leading to the low RMS roughness of 0.163 (Fig. 2d). When the Ti/Al concentrations are $Ti_{3.9\ at.\%}/Al_{4.4\ at.\%}$, the very weak crystalline diffraction rings could be distinguished from the SAED (Fig. 2b), but the lattice fringes cannot be found in the TEM micrograph due to the poor crystallinity and low fraction of formed titanium carbide in a-C films which is confirmed by XPS mentioned above (Fig. 1d), and the RMS roughness is 0.358 (Fig. 2e). With the Ti/Al concentrations further increased to $Ti_{8.5\ at.\%}/Al_{14.4\ at.\%}$, the sharp crystalline diffraction rings emerged in Fig. 2c and they are identified to be the (111), (200), (220) and (222) reflections of cubic TiC structure, and the magnified image also reveals the clear lattice fringes of nanoparticles with size of 3—4 nm (noted by the red circles in Fig. 2c) uniformly embedded in the a-C matrix, indicating the existence of nano-crystalline carbide phases and also resulting in the highest roughness of 0.671 (Fig. 2f). This is in agreement with the obtained XPS results (Fig. 1).

The carbon atomic bonding structure is also evaluated by Raman spectroscopy, as illustrated in Fig. 3. It clearly shows that for each case there is a broad asymmetric Raman scattering curve ranged from 1000 to 1700 cm^{-1} (Fig. 3a), suggesting the typical characteristics of a-C film [1]; the intensity of Raman spectra with Ti/Al concentrations decreases gradually, because of the increasing of centrosymmetric phases, such as TiC, aluminum oxidation, which are inactive to the Raman excitation. In general, the Raman spectra can be fitted into two Gaussian peaks including D peak at 1350 cm^{-1} and G peak at 1580 cm^{-1} (Fig. 3b), where the G peak originates from the stretching mode of sp^2 atoms in both aromatic

Table 1
Thickness and compositions of the films deposited at different sputtering currents.

Sputtering current (A)	Thickness (nm)	Deposition rate (nm/min)	Atomic composition (at.%)		
			Ti	Al	C
1.0	702	11.7	0	0	100
1.5	862	14.4	0.4	0	99.6
2.0	1166	19.4	1.3	2.6	96.1
2.5	1237	20.6	3.9	4.4	91.7
3.0	1313	21.9	3.9	7.3	88.8
4.0	1371	22.8	8.5	14.4	77.1

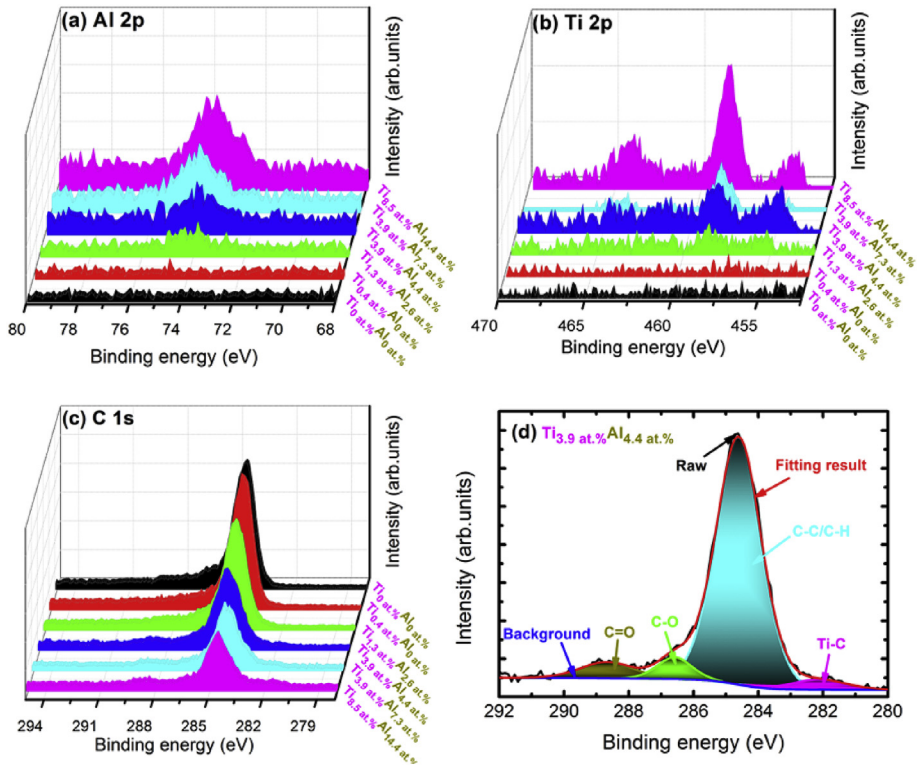

Fig. 1. Typical XPS spectra of the films with different Ti/Al concentrations: (a) Al 2*p*, (b) Ti 2*p*, (c) C1*s*, and (d) the deconvolution of XPS C1*s* peak for the $Ti_{3.9\ at.\%}/Al_{4.4\ at.\%}$ co-doped film. (A colour version of this figure can be viewed online.)

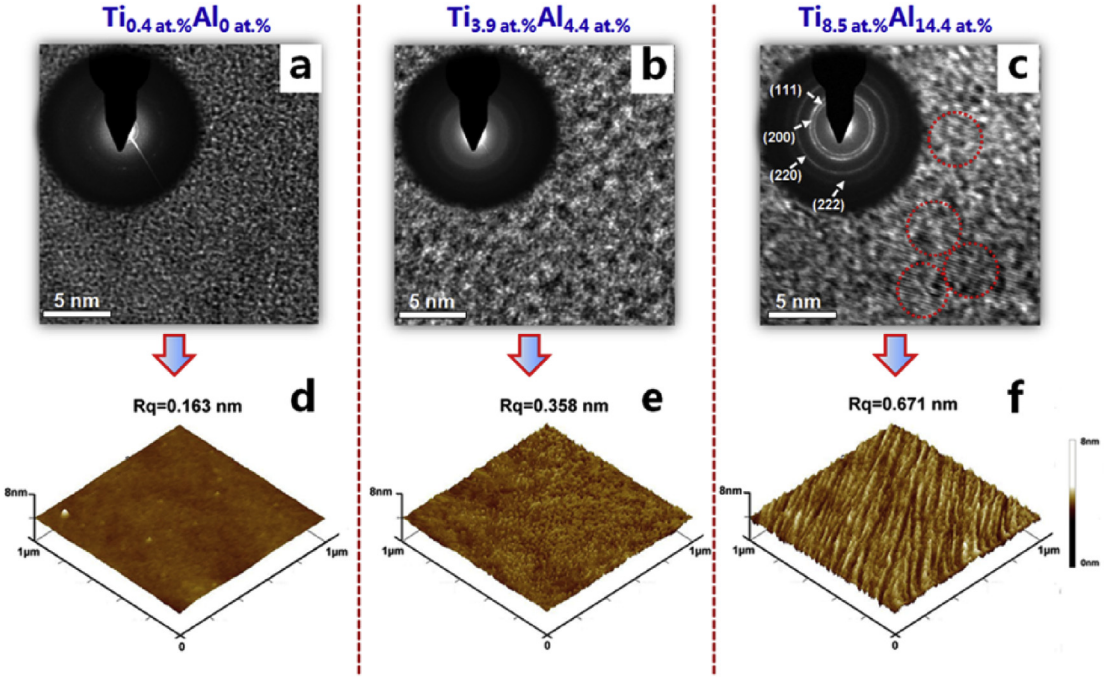

Fig. 2. (a) Cross-sectional TEM micrograph and corresponding SAED pattern; (b) AFM images and the RMS surface roughness of the films with different Ti/Al concentrations of (a) $Ti_{0.4\ at.\%}/Al_{0\ at.\%}$, (b) $Ti_{3.9\ at.\%}/Al_{4.4\ at.\%}$, and (c) $Ti_{8.5\ at.\%}/Al_{14.4\ at.\%}$, respectively. (A colour version of this figure can be viewed online.)

rings and chains, while the D peak is due to the breathing mode of only sp^2 atoms in aromatic rings [1].

The intensity ratio of D peak to G peak, I_D/I_G, and G peak position can be used to evaluate the carbon atomic structure, as shown in Fig. 3c and d. With increasing the Ti/Al concentrations, both the I_D/I_G and G peak position increase first and then decrease; when the Ti/Al concentrations are $Ti_{3.9\ at.\%}/Al_{4.4\ at.\%}$, the maximal values of I_D/I_G and G peak position reach to 1.32 and 1553.6 cm^{-1}, respectively.

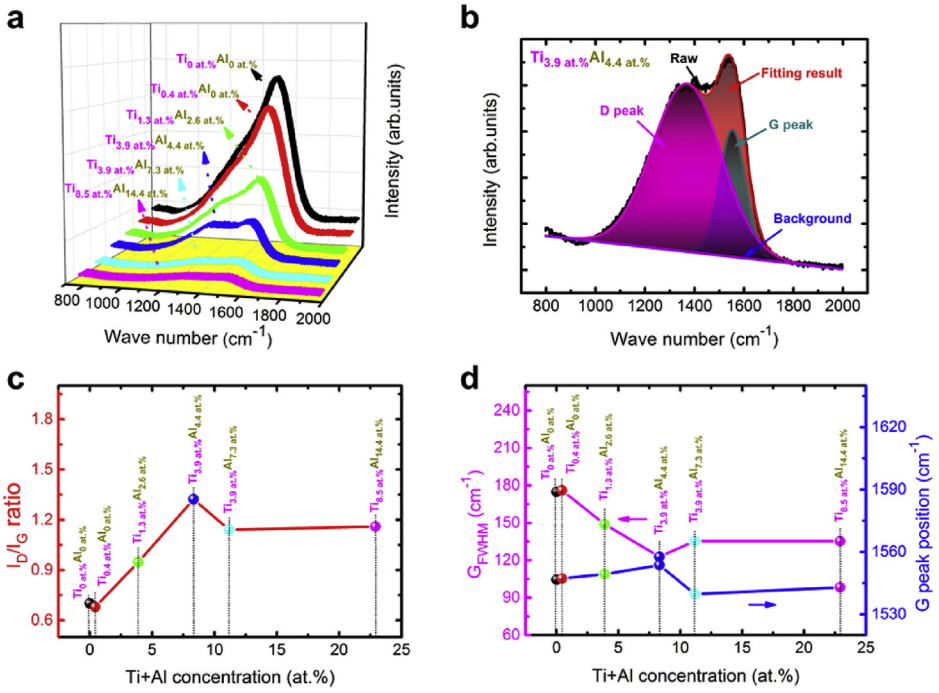

Fig. 3. (a) Raman spectra of the films with different Ti/Al concentrations; (b) the fitted result of Raman spectrum for the $Ti_{3.9\ at.\%}/Al_{4.4\ at.\%}$ co-doped film; (c) corresponding I_D/I_G ratio and (d) FWHM and position of G peak as function of Ti/Al concentrations. (A colour version of this figure can be viewed online.)

It is empirically known that the I_D/I_G increases and G peak position shifts upwards as the increase of graphitic component in the a-C film. The observation in our films reveals that the sp^2 content increases at first and follows by a decrease by changing the Ti/Al concentrations from $Ti_{0\ at.\%}/Al_{0\ at.\%}$ to $Ti_{8.5\ at.\%}/Al_{14.4\ at.\%}$. In addition, Fig. 3d shows that the full width at half maximum of the G peak (G_{FWHM}) decrease monotonously as the Ti/Al concentrations changes from $Ti_{0\ at.\%}/Al_{0\ at.\%}$ to $Ti_{3.9\ at.\%}/Al_{4.4\ at.\%}$, indicating the enhanced ordering and graphitizing of a-C films [35], and then it increases gradually with further increasing the Ti/Al concentrations to $Ti_{8.5\ at.\%}/Al_{14.4\ at.\%}$. This results is consistent with the reports by Dai et al. [32], where the doped Ti atoms as catalysts not only promoted graphitization of a-C films, but also tended to bond with the sp^2-C due to its lower bonding energy compared with sp^3-C, while the doped Al as ductile element mainly contributes to the increase of sp^2-C [8,24]. Consequently, in the Ti/Al co-doped a-C films, when the Ti/Al concentrations changes from $Ti_{0\ at.\%}/Al_{0\ at.\%}$ to $Ti_{3.9\ at.\%}/Al_{4.4\ at.\%}$, the doped Al and Ti with low concentrations causes the graphitization simultaneously. As the Ti/Al concentrations reach beyond of $Ti_{3.9\ at.\%}/Al_{4.4\ at.\%}$, although doping Al promotes the increase of sp^2-C content, Ti atoms with higher concentration could bond with many sp^2-C atoms to form the nano-crystalline carbides, inducing the reduction of sp^2-C content markedly.

3.3. Mechanical properties

Fig. 4 shows the mechanical properties including hardness and elastic modulus. With increasing the Ti/Al concentrations, the hardness and elastic modulus decrease linearly and then increase; the minimal hardness of 13.1 ± 0.3 GPa and elastic modulus of 140 ± 1.4 GPa are obtained as the Ti/Al concentrations are $Ti_{3.9\ at.\%}/Al_{4.4\ at.\%}$. Noted that the mechanical properties of a-C films are mainly dependent on the sp^3 hybridized carbon matrix. According to the Raman and XPS results, the films tend to be graphitizated as

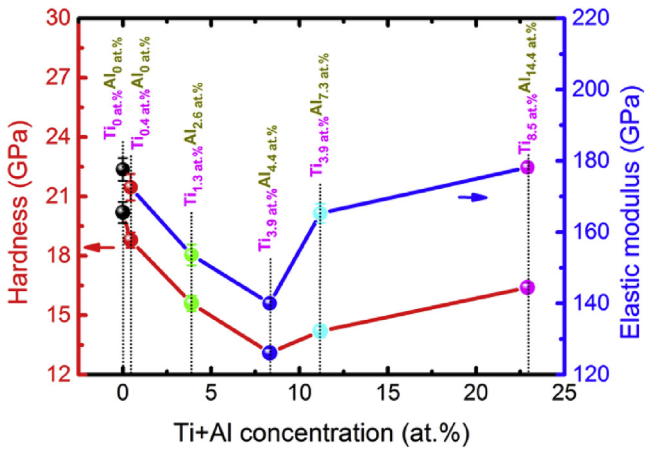

Fig. 4. Hardness and elastic modulus of the Ti/Al co-doped a-C films as a function of Ti/Al concentrations. (A colour version of this figure can be viewed online.)

the Ti/Al concentrations change from $Ti_{0\ at.\%}/Al_{0\ at.\%}$ to $Ti_{3.9\ at.\%}/Al_{4.4\ at.\%}$, resulting in the reduction of hardness obviously. However, when the Ti/Al concentrations are higher than $Ti_{3.9\ at.\%}/Al_{4.4\ at.\%}$, the hard titanium carbide nano-particles are generated due to the increased Ti concentration following the decrease of sp^2 content, which contributes to the increase of the hardness. So the film with $Ti_{8.5\ at.\%}/Al_{14.4\ at.\%}$ shows higher hardness of 16.4 ± 0.3 GPa and elastic modulus of 178 ± 1.4 GPa than that with $Ti_{3.9\ at.\%}/Al_{4.4\ at.\%}$.

Fig. 5 shows the measured residual compressive stress of the films as a function of the Ti/Al concentrations. For comparison, the change of residual stress per thickness as a function of Ti/Al concentrations is also given as Fig. S3 in Supporting Information, revealing that the film thickness has no significant effect on the evolution trend of residual stress with Ti/Al concentrations. As the Ti/Al concentrations increase up to $Ti_{3.9\ at.\%}/Al_{4.4\ at.\%}$ from $Ti_{0\ at.\%}/Al_0$

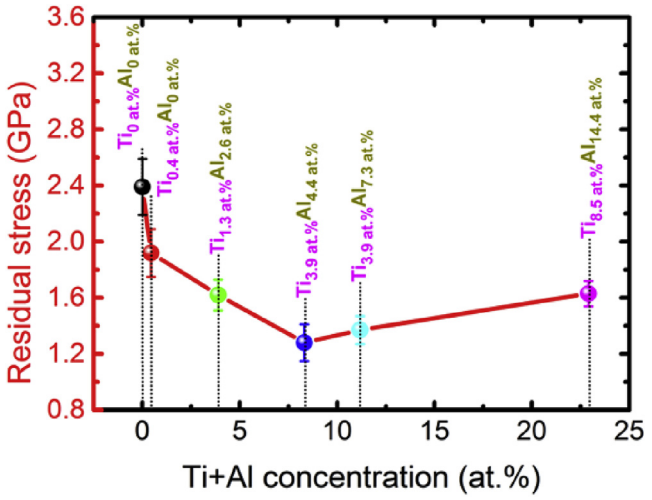

Fig. 5. Residual stress of the Ti/Al co-doped a-C films as a function of Ti/Al concentrations. (A colour version of this figure can be viewed online.)

at.%, the compressive stress of the film dramatically drops down to 1.28 ± 0.13 from 2.39 ± 0.20 GPa, whereas it subsequently increases to 1.63 ± 0.09 GPa as the Ti/Al concentrations reach to $Ti_{8.5\ at.\%}/Al_{14.4\ at.\%}$, which shows the similar behavior with the Ti mono-doped case [32]. Compared with the $Ti_{0\ at.\%}/Al_{0\ at.\%}$ co-doped film, the compressive stress reduces by 46% maximally. According to the above structural and composition analysis, when the Ti/Al concentrations are less than $Ti_{3.9\ at.\%}/Al_{4.4\ at.\%}$, the co-doped Ti/Al atoms are uniformly dissolved in the amorphous carbon matrix and no nano-crystalline carbides emerged. Especially, previous works have proposed that the doped Ti could play a pivot site of metal nano-crystallites for structure relaxation [32], while Al could promote graphitization of C sp^2 bonds [8], which result in the reduction of residual stress. The $Ti_{3.9\ at.\%}/Al_{4.4\ at.\%}$ co-doped a-C film, therefore, presents the minimal residual stress. With increasing the Ti/Al concentrations to $Ti_{8.5\ at.\%}/Al_{14.4\ at.\%}$, the formation of the hard titanium carbide phase makes a dominated contribution to the increase of residual compressive stress [32]. Nevertheless, this is limited to the phenomenological explanation for stress reduction mechanism, the fundamental understanding based on atomic and electronic bond structure is still required.

3.4. Atomic and electronic bond structure analysis

In order to elucidate the properties in terms of the doped metal concentrations and provide further insight to the stress reduction mechanism, ab initio calculations were carried out to provide more direct evidences for the atomic structure and chemical states of Ti/Al co-doped a-C films. During ab initio calculations, the Ti/Al concentrations were selected ranging from $Ti_{1.7\ at.\%}/Al_{3.3\ at.\%}$, $Ti_{3.3\ at.\%}/Al_{5.0\ at.\%}$ to $Ti_{3.3\ at.\%}/Al_{6.7\ at.\%}$, accordingly corresponding to the $Ti_{1.3\ at.\%}/Al_{2.6\ at.\%}$, $Ti_{3.9\ at.\%}/Al_{4.4\ at.\%}$ or $Ti_{3.9\ at.\%}/Al_{7.3\ at.\%}$ co-doped cases in experiment, and the final structures of Ti/Al co-doped a-C films by ab initio calculations are shown in Fig. 6. The residual stress in modeled Ti/Al co-doped a-C films is computed by the equations shown in previous work [19]. Fig. 7 shows the comparative result of residual stress in Ti/Al co-doped a-C films from experiments and ab initio calculations. It can be seen that the evolutions of residual stress obtained from ab initio calculations as a function of Ti, Al and Ti + Al concentrations are consistent well with those from the experiments, implying that the simulated films could represent the experimental cases to explore the residual stress reduction

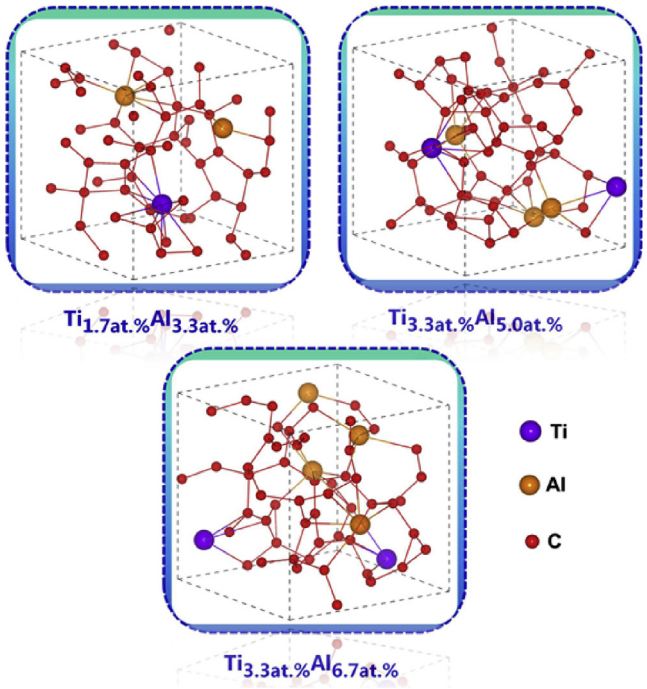

Fig. 6. Atomic structures of Ti/Al co-doped a-C films with different Ti/Al concentrations, in which the number is the concentration of each doped metal atoms. (A colour version of this figure can be viewed online.)

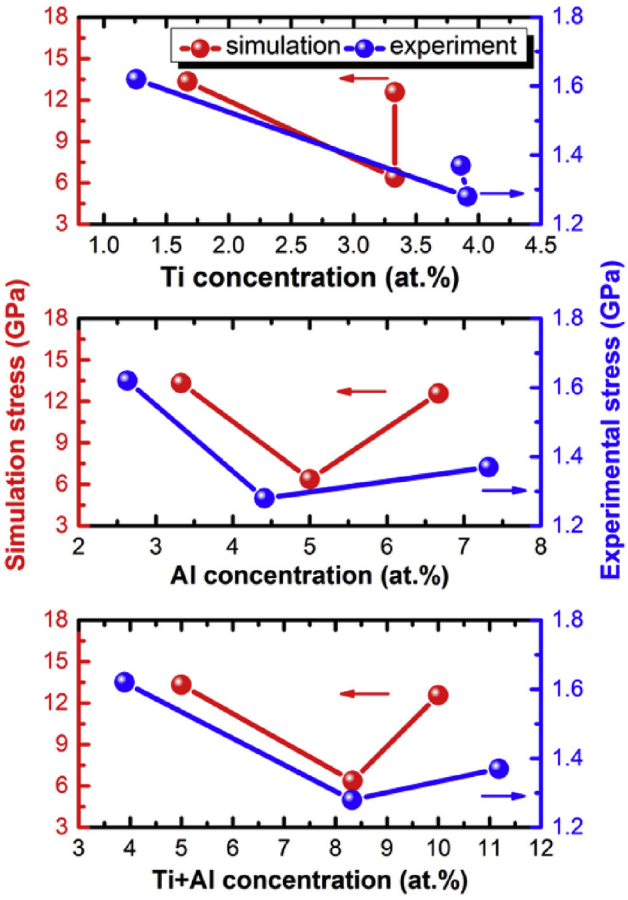

Fig. 7. Comparative result of residual stress in Ti/Al co-doped a-C films from experiments and ab initio calculations. (A colour version of this figure can be viewed online.)

mechanism.

The bond angle and bond length distributions are analyzed firstly to evaluate the change of atomic bond structure caused by co-doped Ti/Al. Previous report [36] has revealed that the high residual compressive stress of a-C films is mainly originated from the distortion of both the bond angles and bond lengths of carbon network, which are less than 109.5° and 1.42 Å, respectively. In order to gain the fractions of distorted bond structures, both the C–C–C bond angle and C–C bond length distributions are calculated, which are presented in Fig. 8a and b, respectively. By integrating the bond angle and bond length distributions (shaded area in Fig. 8), the fractions of distorted bond angles (<109.5°) and bond lengths (<1.42 Å) of carbon network are shown in Fig. 9. It clearly demonstrates that by co-doping $Ti_{1.7\ at.\%}/Al_{3.3\ at.\%}$ into a-C film, the fractions of distorted bond angles and bond lengths are 34.7% and 29.3% separately. Nevertheless, in $Ti_{3.3\ at.\%}/Al_{5.0\ at.\%}$ co-doped a-C films, although the fraction of distorted bond angles slightly increases to 37.3%, the fraction of distorted bond lengths is significantly decreased to 16.2%, which contributes to the drastic reduction of residual stress. With the Ti/Al concentrations further increased to $Ti_{3.3\ at.\%}/Al_{6.7\ at.\%}$, the fraction of distorted bond lengths greatly increases to 25.7% compared to that in $Ti_{3.3\ at.\%}/Al_{5.0\ at.\%}$ co-doped case, leading to the increase of residual stress consequently.

Furthermore, the chemical bonding states caused by Ti/Al co-doping are also illustrated. The density of states reveals the highest occupied molecular orbital (HOMO) mainly being composed of Ti 3*d*, Al 3*p* and C 2*p* atomic orbitals (see Fig. S4 in Supporting Information). Fig. 10 gives the contour plots of charge density of HOMO in the $Ti_{3.3\ at.\%}/Al_{5.0\ at.\%}$ co-doped a-C film representatively which pass through Ti–C or Al–C bond, respectively. It can be seen that the typical characteristic of covalent bond between Ti and C atoms is observed, but the bond strength is much weaker than that of pure C–C bond due to the smaller charge accumulation between Ti and C atoms. Meanwhile, the charge between Al and C atoms in the HOMO shifts to be around the C atom, displaying the ionic feature for Al–C bond [37].

Therefore, it could be concluded that the co-doped Ti/Al atoms in a-C films could form the weak covalent for Ti–C and ionic bond for Al–C separately, which synergistically play the role of a pivotal site to reduce the bond strength and directionality drastically, resulting in the easier distortion of atomic bond structure without inducing the significant increase of strain energy [37]. On the other hand, the highly distorted C–C bond lengths can be relaxed effectively due to the Ti/Al co-doping. As a consequence, these two factors are supposed to be the fundamental reasons why the residual stress of $Ti_{3.9\ at.\%}/Al_{4.4\ at.\%}$ co-doped a-C film in experiment is significantly decreased.

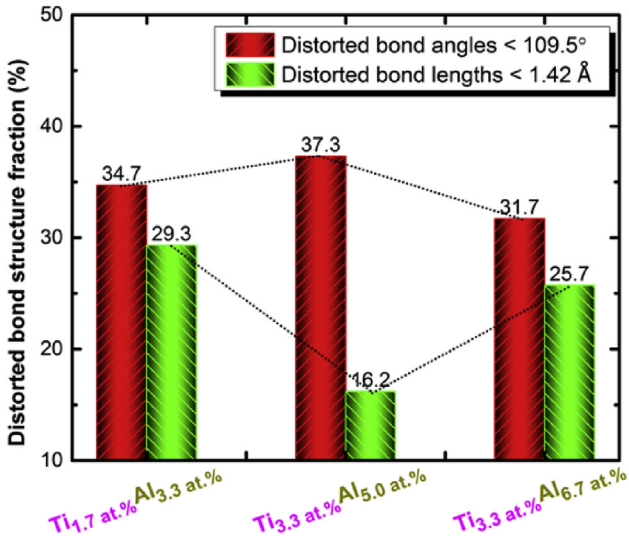

Fig. 9. Fractions of distorted bond angles (<109.5°) and bond lengths (<1.42 Å) in $Ti_{1.7\ at.\%}/Al_{3.3\ at.\%}$, $Ti_{3.3\ at.\%}/Al_{5.0\ at.\%}$ or $Ti_{3.3\ at.\%}/Al_{6.7\ at.\%}$ co-doped a-C films. (A colour version of this figure can be viewed online.)

4. Conclusions

Ti/Al co-doped a-C films were successfully fabricated using a hybrid ion beam system composed of a DC magnetron sputtering source and a linear ion beam hydrocarbon source. Of particular, the residual stress reduction mechanism caused by Ti/Al co-doping was clarified by comprehensive investigation of ab initio calculation and experimental study. Results indicated that Ti/Al co-doping played a significant role on the structure and properties of the films. As the Ti/Al concentrations were smaller than $Ti_{3.9\ at.\%}/Al_{4.4\ at.\%}$, the co-doped Ti/Al atoms were uniformly dissolved in the amorphous carbon matrix promoting the graphitization of the structures, which caused the gradual decrease of mechanical properties and residual stress. Specifically, the minimal residual stress of 1.28 ± 0.13 GPa was obtained in the $Ti_{3.9\ at.\%}/Al_{4.4\ at.\%}$ co-doped a-C film. When the Ti/Al concentrations increased beyond of $Ti_{3.9\ at.\%}$/

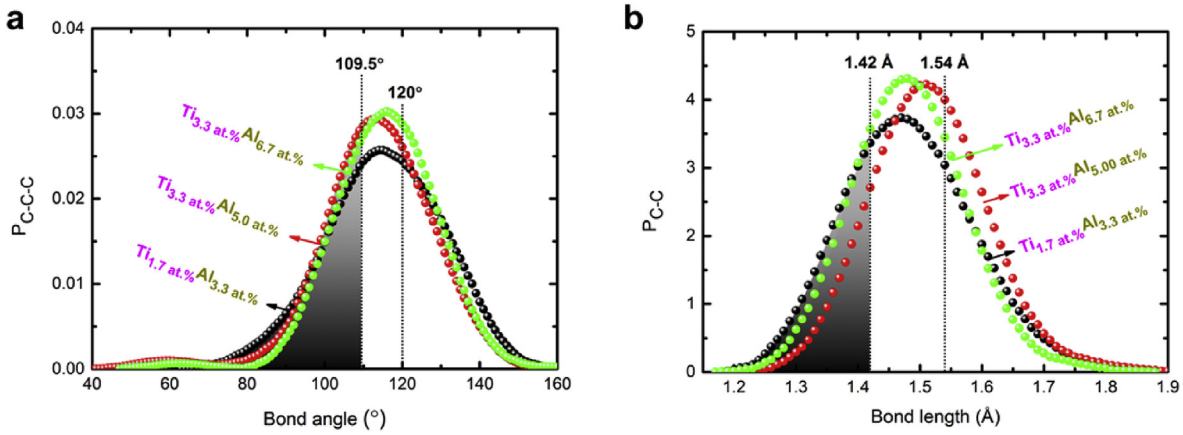

Fig. 8. Atomic bond structure of Ti/Al co-doped a-C films. (a) bond angle distributions of C–C–C, P_{C-C-C}, in which the black vertical dotted lines represent the stable bond angles of 120° for graphite and the one of 109.5° for diamond. (b) bond length distributions of C–C, P_{C-C}, in which the red vertical dotted lines represent the stable bond lengths of 1.42 Å and 1.54 Å for stable sp^2 and sp^3 C–C bonds, respectively. (A colour version of this figure can be viewed online.)

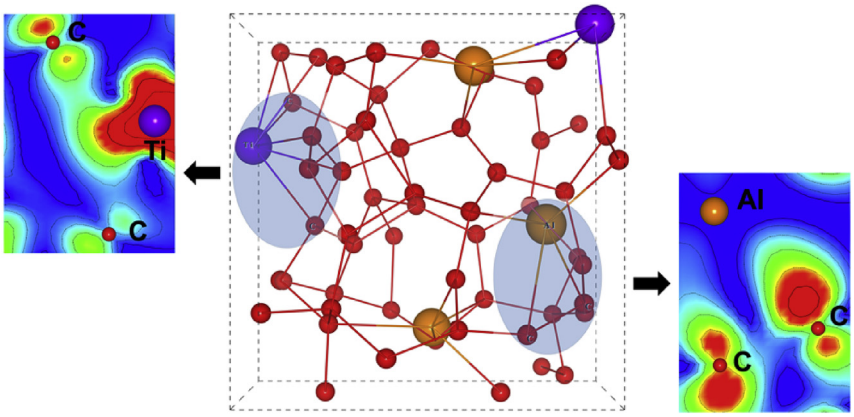

Fig. 10. Contour plots of charge density of HOMO passing through Ti–C or Al–C bond, respectively, in the $Ti_{3.3\ at.\%}/Al_{5\ at.\%}$ co-doped a-C film. (A colour version of this figure can be viewed online.)

$Al_{4.4\ at.\%}$ to $Ti_{8.5\ at.\%}/Al_{14.4\ at.\%}$, the doped Ti atoms were involved to bond with C atoms forming the hard carbide phases, while Al atoms existed in the form of aluminum oxidation phases, which were all embedded in the a-C matrix, inducing the higher hardness of the films. The analysis of atomic bond structure and bond characteristics by ab initio calculations revealed that co-doping Ti/Al into a-C films could not only relax the distorted C–C bond lengths, but also forms the weak covalent bond for Ti–C and ionic bond for Al–C, respectively. This accounted for the obvious residual stress reduction observed in experimental case of $Ti_{3.9\ at.\%}/Al_{4.4\ at.\%}$ co-doped a-C film. Most of important result presented here is that the relationship between microstructures and mechanical properties of binary metal co-doped carbon functional materials is addressed for the carbon communities, which is thought to be a novel concept to design and tailor the nanostructured carbon materials with comprehensive mechanical and wear-corrosion performance for harsh protective applications.

Acknowledgments

This research was supported by State Key Project of Fundamental Research of China (2013CB632302), National Natural Science Foundation of China (51402319, 51522106), and the project of International Cooperation Foundation (2015D10004) of Ningbo Government.

Appendix A. Supplementary data

Supplementary data related to this article can be found at http://dx.doi.org/10.1016/j.carbon.2016.10.033.

References

[1] J. Robertson, Diamond-like amorphous carbon, Mater. Sci. Eng. 37 (4–6) (2002) 129–281.
[2] J. Wang, J. Pu, G. Zhang, L. Wang, Interface architecture for superthick carbon-based films toward low internal stress and ultrahigh load-bearing capacity, ACS Appl. Mater. Interfaces 5 (11) (2013) 5015–5024.
[3] K. Bewilogua, D. Hofmann, History of diamond-like carbon films—from first experiments to worldwide applications, Surf. Coat. Technol. 242 (2014) 214–225.
[4] H.S. Hsu, P.E. Lu, C.W. Chang, S.J. Sun, C.H. Lee, H.C. Su, Y.Y. Chin, H.J. Lin, C.T. Chen, M.J. Huang, Tunable interfacial magnetic-optical properties of Co doped amorphous carbon film induced by charge transfer after acid treatment, Carbon 77 (2014) 398–404.
[5] N. Dwivedi, S. Kumar, J.D. Carey, R.K. Tripathi, H.K. Malik, M.K. Dalai, Influence of silver incorporation on the structural and electrical properties of diamond-like carbon thin films, ACS Appl. Mater. Interfaces 5 (7) (2013) 2725–2732.
[6] J. Huang, L. Wang, B. Liu, S. Wan, Q. Xue, In vitro evaluation of the tribological response of Mo-doped graphite-like carbon film in different biological media, ACS Appl. Mater. Interfaces 7 (4) (2015) 2772–2783.
[7] A.Y. Wang, K.R. Lee, J.P. Ahn, J.H. Han, Structure and mechanical properties of W incorporated diamond-like carbon films prepared by a hybrid ion beam deposition technique, Carbon 44 (2006) 1826–1832.
[8] W. Dai, A.Y. Wang, Deposition and properties of Al-containing diamond-like carbon films by a hybrid ion beam sources, J. Alloys Compd. 509 (13) (2011) 4626–4631.
[9] C.S. Lee, K.R. Lee, K.Y. Eun, K.H. Yoon, J.H. Han, Structure and properties of Si incorporated tetrahedral amorphous carbon films prepared by hybrid filtered vacuum arc process, Diam. Relat. Mater. 11 (2) (2002) 198–203.
[10] A.Y. Wang, H.S. Ahn, K.R. Lee, J.P. Ahn, Unusual stress behavior in W-incorporated hydrogenated amorphous carbon films, Appl. Phys. Lett. 86 (11) (2005), 111902-1–3.
[11] K. Baba, R. Hatada, Deposition and characterization of Ti- and W-containing diamond-like carbon films by plasma source ion implantation, Surf. Coat. Technol. 169–170 (2003) 287–290.
[12] G. Zhang, P. Yan, P. Wang, Y. Chen, J. Zhang, The preparation and mechanical properties of Al-containing a-C: H thin films, J. Phys. D. Appl. Phys. 40 (21) (2007) 6748–6752.
[13] H. Nakazawa, R. Kamata, S. Okuno, Deposition of silicon-doped diamond-like carbon films by plasma-enhanced chemical vapor deposition using an intermittent supply of organosilane, Diam. Relat. Mater. 51 (2015) 7–13.
[14] D. Batory, J. Gorzedowski, B. Rajchel, L. Szymanski, L. Kolodziejczyk, Silver implanted diamond-like carbon coatings, Vacuum 110 (2014) 78–86.
[15] X. Pang, J. Hao, P. Wang, Y. Xia, W. Liu, Effects of bias voltage on structure and properties of TiAl-doped a-C: H films prepared by magnetron sputtering, Surf. Interface Anal. 43 (2011) 677–682.
[16] X. Pang, L. Shi, P. Wang, Y. Xia, W. Liu, Effects of Al incorporation on the mechanical and tribological properties of Ti-doped a-C: H films deposited by magnetron sputtering, Curr. Appl. Phys. 11 (2011) 771–775.
[17] X. Liu, J. Yang, J. Hao, J. Zheng, Q. Gong, W. Liu, A near-frictionless and extremely elastic hydrogenated amorphous carbon film with self-assembled dual nanostructure, Adv. Mater. 24 (34) (2012) 4614–4617.
[18] R. Zhang, L. Wang, Z. Lu, Probing the intrinsic failure mechanism of fluorinated amorphous carbon film based on the first-principles calculation, Sci. Rep. 5 (2015), 9419–1–9.
[19] X. Li, P. Ke, A. Wang, Probing the stress reduction mechanism of diamond-like carbon films by incorporating Ti, Cr, or W carbide-forming metals: ab initio molecular dynamics simulation, J. Phys. Chem. C 119 (2015) 6086–6093.
[20] H.W. Strauss, R.R. Chromik, S. Hassani, J.E. Klemberg-Sapieha, In situ tribology of nanocomposite Ti-Si-C-H coatings prepared by PE-CVD, Wear 272 (1) (2011) 133–148.
[21] J.Y. Jao, S. Han, C.C. Yen, Y.C. Liu, L.S. Chang, C.L. Chang, H.C. Shih, Bias voltage effect on the structure and property of the (Ti:Cu)-DLC films fabricated by cathodic arc plasma, Diam. Relat. Mater. 20 (2) (2011) 123–129.
[22] A. Anders, Plasma and ion sources in large area coating: a review, Surf. Coat. Technol. 200 (5–6) (2005) 1893–1906.
[23] I.V. Bordenjuk, O.A. Panchenko, S.V. Sologub, I.G. Brown, Development of additional magnetron discharge in the drift region of an ion source with closed electron drift, Probl. A. T. Sci. Technol. 6 (2008) 168–170.
[24] W. Dai, P. Ke, A. Wang, Influence of bias voltage on microstructure and properties of Al-containing diamond-like carbon films deposited by a hybrid ion beam system, Surf. Coat. Technol. 229 (2013) 217–221.
[25] W. Dai, A. Wang, Synthesis, characterization and properties of the DLC films with low Cr concentration doping by a hybrid linear ion beam system, Surf. Coat. Technol. 205 (8–9) (2011) 2882–2886.
[26] G. Kresse, J. Furthmüller, Efficiency of ab initio total energy calculations for metals and semiconductors using plane-wave basis set, Comput. Mater. Sci. 6

(1) (1996) 15–50.
[27] G. Kresse, J. Furthmüller, Efficient iterative schemes for ab initio total-energy calculations using a plane-wave basis set, Phys. Rev. B 54 (16) (1996) 11169–11186.
[28] D.G. McCulloch, D.R. McKenzie, C.M. Goringe, Ab initio simulations of the structure of amorphous carbon, Phys. Rev. B 61 (3) (2000) 2349–2355.
[29] B. Zheng, W.T. Zheng, K. Zhang, Q.B. Wen, J.Q. Zhu, S.H. Meng, X.D. He, J.C. Han, First-principle study of nitrogen incorporation in amorphous carbon, Carbon 44 (5) (2006) 962–968.
[30] M.M.M. Bilek, D.R. McKenzie, D.G. McCulloch, C.M. Goringe, Ab initio simulation of structure in amorphous hydrogenated carbon, Phys. Rev. B 62 (5) (2000) 3071–3077.
[31] J.P. Perdew, K. Burke, M. Ernzerhof, Generalized gradient approximation made simple, Phys. Rev. Lett. 77 (18) (1996) 3865–3868.
[32] W. Dai, P. Ke, M. Moon, K.R. Lee, A. Wang, Investigation of the microstructure, mechanical properties and tribological behaviors of Ti-containing diamond-like carbon films fabricated by a hybrid ion beam method, Thin Solid Films 520 (19) (2012) 6057–6063.
[33] D. Bourgoin, S. Turgeon, G.G. Ross, Characterization of hydrogenated amorphous carbon films produced by plasma-enhanced chemical vapour deposition with various chemical hybridizations, Thin Solid Films 357 (2) (1999) 246–253.
[34] B.K. Tay, P. Zhang, On the properties of nanocomposite amorphous carbon films prepared by off-plane double bend filtered cathodic vacuum arc, Thin Solid Films 420–421 (2002) 177–184.
[35] C. Casiraghi, A.C. Ferrari, J. Robertson, Raman spectroscopy of hydrogenated amorphous carbons, Phys. Rev. B 72 (8) (2005), 085401-1–14.
[36] X. Li, P. Ke, H. Zheng, A. Wang, Structural properties and growth evolution of diamond-like carbon films with different incident energies: a molecular dynamics study, Appl. Surf. Sci. 273 (2013) 670–675.
[37] J.H. Choi, S.C. Lee, K.R. Lee, A first-principles study on the bond characteristics in carbon containing Mo, Ag, or Al impurity atoms, Carbon 46 (2008) 185–188.